nature genetics

Mutations in *INPP5E*, encoding inositol polyphosphate-5-phosphatase E, link phosphatidyl inositol signaling to the ciliopathies

Stephanie L Bielas[1,18], Jennifer L Silhavy[1,18], Francesco Brancati[2,3,18], Marina V Kisseleva[4,18], Lihadh Al-Gazali[5,18], Laszlo Sztriha[6], Riad A Bayoumi[7], Maha S Zaki[8], Alice Abdel-Aleem[9], Rasim Ozgur Rosti[10], Hulya Kayserili[10], Dominika Swistun[1], Lesley C Scott[1], Enrico Bertini[11], Eugen Boltshauser[12], Elisa Fazzi[13], Lorena Travaglini[2], Seth J Field[14], Stephanie Gayral[15], Monique Jacoby[15], Stephane Schurmans[15], Bruno Dallapiccola[2,16], Philip W Majerus[4], Enza Maria Valente[2,17] & Joseph G Gleeson[1]

Phosphotidylinositol (PtdIns) signaling is tightly regulated both spatially and temporally by subcellularly localized PtdIns kinases and phosphatases that dynamically alter downstream signaling events[1]. Joubert syndrome is characterized by a specific midbrain-hindbrain malformation ('molar tooth sign'), variably associated retinal dystrophy, nephronophthisis, liver fibrosis and polydactyly[2] and is included in the newly emerging group of 'ciliopathies'. In individuals with Joubert disease genetically linked to *JBTS1*, we identified mutations in the *INPP5E* gene, encoding inositol polyphosphate-5-phosphatase E, which hydrolyzes the 5-phosphate of PtdIns(3,4,5)P3 and PtdIns(4,5)P2. Mutations clustered in the phosphatase domain and impaired 5-phosphatase activity, resulting in altered cellular PtdIns ratios. INPP5E localized to cilia in major organs affected by Joubert syndrome, and mutations promoted premature destabilization of cilia in response to stimulation. These data link PtdIns signaling to the primary cilium, a cellular structure that is becoming increasingly recognized for its role in mediating cell signals and neuronal function.

Joubert syndrome locus 1 (*JBTS1*, MIM%213300) was mapped to the distal q-arm of chromosome 9, between D9S1826 and D9S1838, in two Emirate families variably associated with retinopathy and a proven 'molar tooth' sign (MTI-007 and MTI-008, previously called families A and C, respectively; **Fig. 1a** and **Supplementary Table 1**)[3]. To refine the candidate interval, we recruited two additional unaffected MTI-007 family members and two affected MTI-008 family members and performed a 5K SNP analysis, confirming linkage to *JBTS1* in MTI-007 (**Supplementary Fig. 1**). Family MTI-008 produced a linkage peak at *JBTS1*, among several other peaks of similar amplitude, with a maximum lod score of about +1.94. As a result, these SNP scans failed to significantly narrow the candidate interval (**Supplementary Table 2**).

We analyzed an additional 25 consanguineous families with Joubert syndrome, and three (MTI-134, MTI-610 and MTI-627, of Emirate, Turkish and Egyptian descent, respectively) showed at least one peak that overlapped with *JBTS1*. Two Italian families (COR-10 and COR-21) were also linked to *JBTS1* (ref. 4). Haplotype analysis suggested that MTI-007 and MTI-134 were identical by descent, as were COR-10 and COR-21 (data not shown). Together, these analyses defined a candidate interval of 3.5 Mb in distal 9q34.2-tel containing approximately 86 annotated candidate genes (**Supplementary Table 3**), of which we screened 57 for sequence changes. The remaining 29 either lacked an open reading frame or were excluded because of lack of developmental expression. This extensive screening identified the *INPP5E* gene as mutated in each *JBTS1*-linked family (**Fig. 1a**,**b**).

The *INPP5E* mutations were notable for two reasons. First, all identified mutations caused missense changes that clustered within

[1]Neurogenetics Laboratory, Howard Hughes Medical Institute, Department of Neurosciences and Pediatrics, University of California, San Diego, La Jolla, USA. [2]Casa Sollievo della Sofferenza-Mendel Institute, Casa Sollievo della Sofferenza Hospital, Rome, Italy. [3]Department of Biomedical Sciences and Aging Research Center, Centro Studi sull'Invecchiamento, G. d'Annunzio University Foundation, Chieti, Italy. [4]Division of Hematology, Department of Internal Medicine, Washington University School of Medicine, St. Louis, Missouri, USA. [5]Departments of Pediatrics and Pathology, United Arab Emirates University, Faculty of Medicine and Health Sciences, Al Ain, United Arab Emirates. [6]Department of Pediatrics, University of Szeged, Szeged, Hungary. [7]College of Medicine, Sultan Qaboos University, Al-Khoud, Sultanate of Oman. [8]Clinical Genetics Department and [9]Medical Molecular Genetics Department, Human Genetics and Genome Research Division, National Research Centre, Dokki, Cairo, Egypt. [10]Istanbul University, Istanbul Medical Faculty, Medical Genetics, Millet Caddesi, Capa, Fatih, Istanbul, Turkey. [11]Unit of Molecular Medicine, Department of Laboratory Medicine, Bambino Gesu Children's Research Hospital, Rome, Italy. [12]Department of Paediatric Neurology, University Children's Hospital of Zurich, Zurich, Switzerland. [13]Department of Child Neurology and Psychiatry, C. Mondino, Pavia, Italy. [14]Division of Endocrinology and Metabolism, Department of Medicine, University of California, San Diego, La Jolla, USA. [15]Institut de Recherche Interdisciplinaire en Biologie Humaine et Moleculaire (IRIBHM), Institut de Biologie et de Médecine Moléculaires (IBMM), Université Libre de Bruxelles, Gosselies, Belgium. [16]Department of Experimental Medicine, Sapienza University, Rome, Italy. [17]Department of Medical and Surgical Paediatric Sciences, University of Messina, Messina, Italy. [18]These authors contributed equally to this work. Correspondence should be addressed to J.G.G. (jogleeson@ucsd.edu).

Received 1 December 2008; accepted 15 June 2009; published online 9 August 2009; doi:10.1038/ng.423

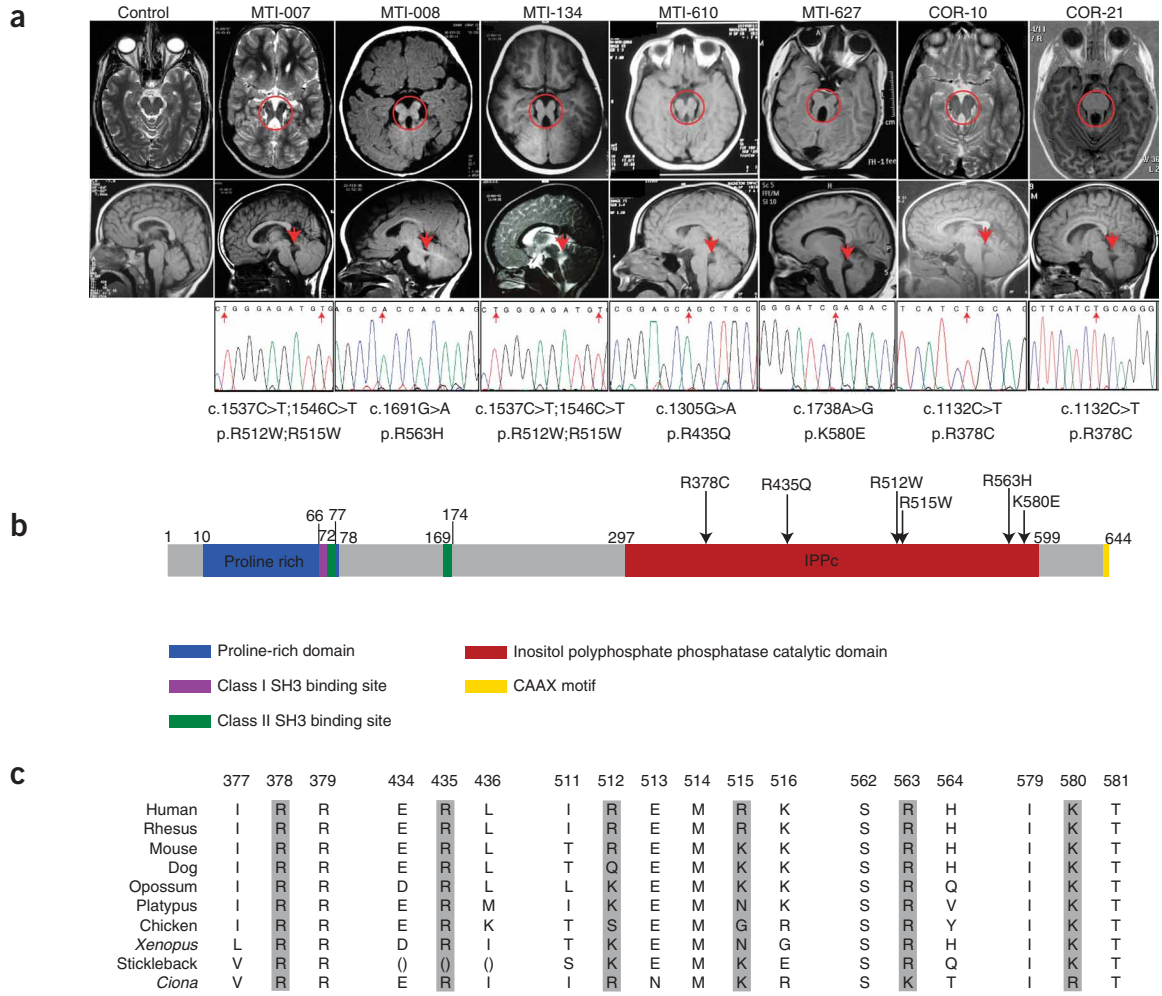

Figure 1 Missense mutations in the encoded enzymatic domain of *INPP5E* (inositol polyphate-5-phosphatase E) in individuals linked to the *JBTS1* locus. (**a**) Top, axial brain MRIs showing molar tooth sign (red circle) from one affected member of each linked family, representing four different countries of origin. Bottom, midline sagittal MRIs showing horizontally oriented superior cerebellar peduncle (red arrow), not evident in control. Below are sequence chromatograms from one affected member of each family, showing the nucleotide change (red arrow) with corresponding amino acid substitution listed below. Families MTI-007 and MTI-134 shared a common haplotype at the *JBTS1* locus, as did COR-10 and COR-21, and they share common mutations. MTI-007 and MTI-134 have a compound homozygous mutation with a double R512W; R515W. (**b**) Predicted protein domains of INPP5E indicated by color. Each of the identified missense mutations (arrows) occurs in a basic residue within the catalytic domain and alters charge. (**c**) Evolutionary conservation of mutant amino acids.

the enzymatically active phosphatase domain (**Fig. 1b**). Second, each altered the charge of highly basic, evolutionarily conserved amino acid residues (**Fig. 1c**). Taken together, these two characteristics suggest that these mutations might alter enzymatic activity. None of these mutations were found among 188 control chromosomes from healthy ethnically matched individuals, and all mutations segregated with the disease in each family. We modeled these mutations using the published crystal structure of synaptojanin[5], the only inositol 5-phosphatase for which structural data are available. We found that each of the altered residues (with the exception of Arg563) was predicted to project its charged tail toward the presumed binding pocket of the PtdIns substrate (**Supplementary Fig. 2**), suggesting that these mutations might alter substrate specificity.

To test the effects of *INPP5E* mutations on PtdIns phosphatase activity, we immunoprecipitated Myc-tagged wild-type, enzymatically null (D477N)[6] and mutant INPP5E, representing each of the patient mutations from mammalian cells (resulting in similar INPP5E protein levels; **Supplementary Fig. 3**) and then analyzed phosphatase activity against PtdIns(3,4,5)P3 and PtdIns(4,5)P2, the presumed cellular INPP5E substrates (**Fig. 2a**). We found that each of the *JBTS1* missense mutations severely disrupted phosphatase activity toward PtdIns(3,4,5)P3 (**Fig. 2b**; $P < 0.05$ compared with wild type for activity values; $n = 3$ independent experiments). Of note, because the R512W and R515W variants were observed on a single haplotype, we reasoned that only one of them was likely to be driving the defect in enzymatic activity; when we analyzed the two variants separately, we found that the R515W substitution was the major contributor to the defective enzymatic activity (data not shown). Comparison of phosphatase activity using PtdIns(4,5)P2 as the substrate showed similar, although less severe, defects in activity as compared to wild-type (**Fig. 2c**), suggesting that PtdIns(3,4,5)P3 may be the relevant substrate in *JBTS1*. Because overexpression of INPP5E was previously shown to block Akt phosphorylation in response to PDGF stimulation in cultured cells (presumably by depleting levels of PtdIns(3,4,5)P3 and

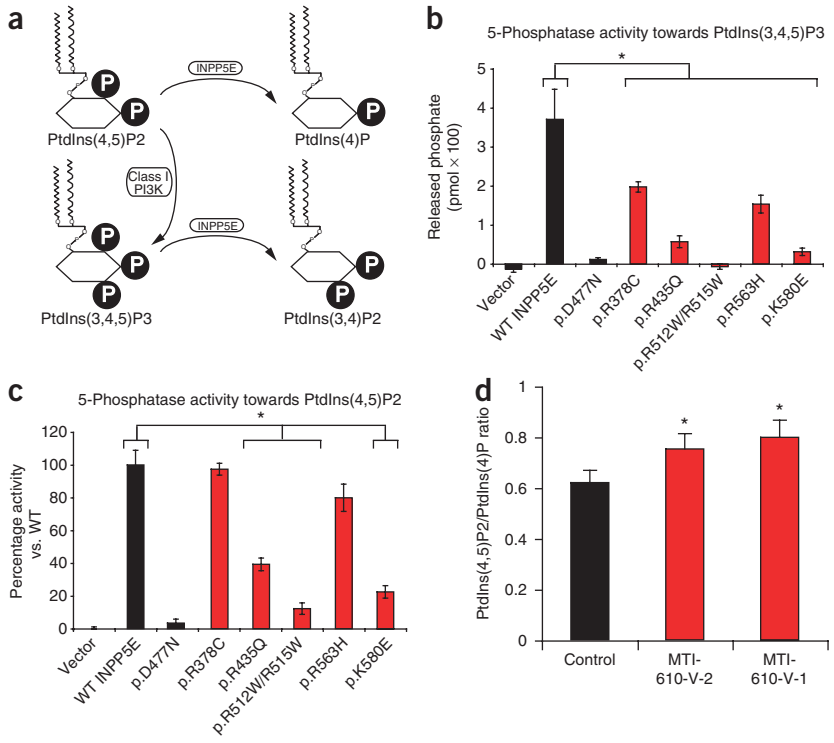

Figure 2 Impaired 5-phosphatase activity and altered ratio of PtdIns(4,5)P2 to PtdIns(4)P associated with *JBTS1 INPP5E* mutations. (**a**) Summary of PtdIns metabolism. *P*, phosphate. A block in INPP5E function is predicted to increase the PtdIns(4,5)P2:PtdIns(4)P ratio. (**b**,**c**) More severe reduction in 5-phosphatase activity of mutant INPP5E against PtdIns(3,4,5)P3 than PtdIns(4,5)P2 substrates. Note that activity was largely retained against PtdIns(4,5)2 for some mutations (mutants R435Q, R512W/R515W and K580E are severely defective, whereas R378C and R563H are only slightly diminished). D477N, a known phosphatase-dead mutant, was compared with each of the *JBTS1* mutations ($n = 3$ for each sample). Error bars, s.e.m. (**d**) Elevated ratio of PtdIns(4,5)P2 to PtdIns(4)P in patient primary fibroblast lines MTI-610-V-2 and V-1 compared with control fibroblast. Error bars, s.d. $^*P < 0.05$, two-way ANOVA corrected for multiple comparisons.

PtdIns(4,5)P2)[7], we next tested the effect of overexpressing each of the *JBTS1*-associated mutations in this published assay. Not only did the mutant proteins fail to block Akt signaling, but elevated basal levels of pAkt were also apparent in unstimulated cells (**Supplementary Fig. 4**). We conclude that the *JBTS1*-associated missense mutations impair phosphatase activity toward putative PtdIns substrates, which can alter downstream signaling events.

Next, we tested whether the absence of endogenous catalytic INPP5E activity results in altered PtdIns profiles in cells. Although it is difficult to measure absolute levels of PtdIns moieties in cells, the model predicted an increased ratio of PtdIns(4,5)P2 to PtdIns(4)P due to a block in this enzymatic step (**Fig. 2a**). Thus, we assessed the PtdIns(4,5)P2/PtdIns(4)P ratio in skin fibroblasts from individuals 1 and 2 of family MTI-610 (a brother and sister). In unstimulated growth-arrested control fibroblasts, we found a PtdIns(4,5)P2/PtdIns(4)P ratio of about 0.63, whereas in both fibroblast samples from the MTI-610 family, the ratio was increased by about 20% ($P = 0.05$; $n = 3$ independent experiments; **Fig. 2d**). We found no differences in the expression levels of INPP5E in these or any other fibroblast samples from individuals with *INPP5E* mutations (**Supplementary Fig. 5**). We conclude that catalytic activity of INPP5E is required to maintain homeostatic ratios of PtdIns in cells.

To investigate a possible connection with ciliopathies, we examined INPP5E localization in cells with well-described cilia. The RPE-hTERT cell line (immortalized retinal pigment epithelium) shows a primary cilium in >80% of growth-arrested cells[8,9]. Coimmunostaining with pericentrin, a marker of the pericentriolar matrix, showed INPP5E immediately adjacent to the base of the cilium (**Fig. 3a**). This was confirmed by INPP5E coimmunostaining with acetylated tubulin, a marker of the ciliary axoneme, as well as with ARL13B, a cilia marker[10–12], which showed tight colocalization of INPP5E to the ciliary axoneme with only minimal INPP5E localized to nonciliary locations (**Fig. 3b**). Transfection of wild-type green fluorescent protein (GFP)-tagged INPP5E into IMCD-3 cells under conditions conducive to cilium formation demonstrated ciliary localization of INPP5E (**Supplementary Fig. 6**), and we found no defect in ciliary localization of any of the *JBTS1*-associated missense mutations when expressed in these cells (data not shown). By contrast, cells at mitotic stages (after

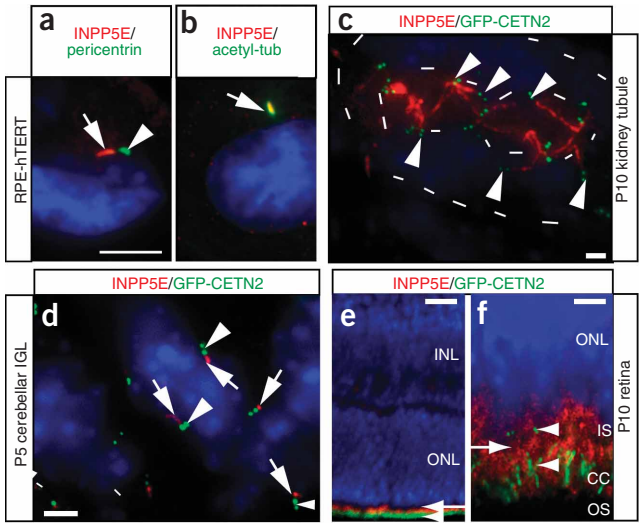

Figure 3 Ciliary axonemal localization of INPP5E. (**a**) RPE-hTERT ciliated cells stained for INPP5E and cilia markers. INPP5E (red, arrow) localized adjacent to pericentrin-positive (green, arrowhead) pericentriolar matrix. (**b**) Colocalization (yellow) of INPP5E (red, arrow) with ciliary axonemal acetylated tubulin (green, arrow). (**c–f**) INPP5E (red) staining in GFP-*Cetn2* transgenic mouse (green pair of centrioles, arrowheads). (**c**) Postnatal day (P) 10 kidney collecting tubule shows INPP5E-positive red cilia projecting into the renal tubule lumen (inner dashes); limits of tubule indicated by outer dashes. (**d**) P5 cerebellar internal granule layer (IGL) with INPP5E (red, arrows) ciliary axoneme adjacent to the centrioles. (**e**) P10 retina, where GFP-CETN2 labels the basal body and connecting cilium (CC, green, arrowhead). INPP5E exclusively labels photoreceptor cells (red, arrow). (**f**) High-power view of **e** showing INPP5E staining (red, arrow) in the inner segment (IS), just adjacent to and above basal bodies and CC (arrowheads). Blue, Hoechst stain. Scale bars, 5 μm (**a**,**b**,**d**), 25 μm (**c**), 50 μm (**e**), 10 μm (**f**). INL, inner nuclear layer; OLN, outer nuclear layer; OS, outer segment.

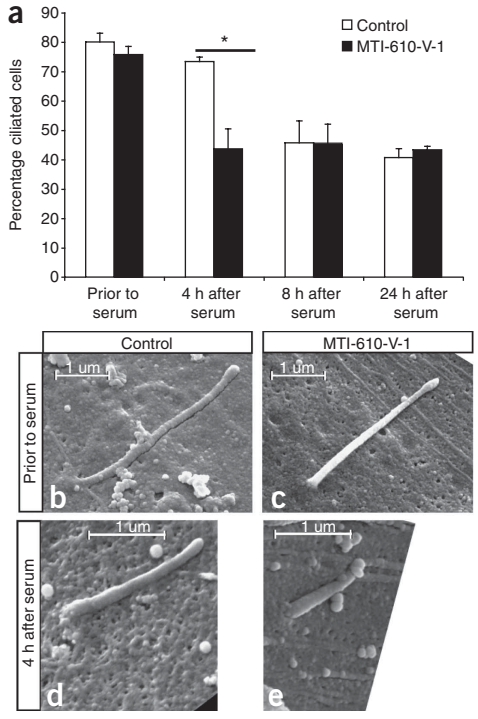

Figure 4 Effects of *INPP5E* mutations on ciliary stability. (**a**) Lability of cilia in MTI-610-V-1 primary fibroblasts with mutant *INPP5E*. Before serum stimulation, serum-starved control and patient fibroblasts showed comparable percentage of ciliated cells. By 4 h after serum stimulation, the ciliated cells dropped to 43% in patient fibroblast as compared to 73% in control (* $P < 0.01$, $n = 3$, total cells counted >250 for each condition). By 8 h or 24 h after stimulation, percentages of ciliated cells were again comparable between MTI-610-V-1 and control samples. Error bars, s.e.m. (**b–e**) Scanning electron micrographs of control versus MTI-610-V-1 primary fibroblast with mutant *INPP5E*. Before serum stimulation, ciliary axonemal length was comparable, although slightly shorter in the MTI-610-V-1 sample. By 4 h after stimulation, axonemal length was shorter in the MTI-610-V1 sample. Scale bar, μm.

cilium withdrawal) showed cytoplasmic localization (**Supplementary Fig. 7**). The data suggest that INPP5E localizes predominantly to the primary cilium during interphase in the cell lines tested.

We stained for INPP5E in organs affected in Joubert syndrome in the GFP-centrin2 (GFP-*Cetn2*) transgenic mouse (which marks the base of the cilium)[13] and identified cilia localization in each. In renal collecting tubules, cilia were evident projecting from the epithelium into the lumen. In the transgenic mouse, many cells were marked by luminal localization of the pair of centrioles, and from this site, the majority of cells had an INPP5E-positive cilium projecting into the lumen (**Fig. 3c**). In the developing cerebellum, cilia have previously been identified on a population of neuroblasts in the cerebellar internal granule layer[14]. We identified these ciliated cells based on GFP signal at the centrioles and identified INPP5E-positive cilia projecting into the parenchyma in the vast majority of these cells (**Fig. 3d**); similar ciliary localization was observed in the hepatic bile ducts (data not shown). We also observed that INPP5E localized to the region adjacent to the basal body and connecting cilium in retinal photoreceptor cells (**Fig. 3e,f**). Therefore, INPP5E is predominantly localized adjacent to or within the cilia in each of the major organs affected in Joubert syndrome.

To assess the potential function of INPP5E at the primary cilium, we used primary fibroblasts from individual V-1 from the MTI-610 family. These cells showed essentially normal growth characteristics and a similar percentage of ciliated cells compared with controls (81% versus 76%, $P > 0.05$; **Fig. 4a**), suggesting that at least in fibroblasts, INPP5E enzymatic activity is not required for ciliogenesis or cilium maintenance. However, the cilium is not a fixed structure and is labile to the application of serum-derived factors such as PDGF[15]. Because serum is a potent activator of the PtdIns pathway in cultured cells, we predicted that the altered PtdIns profile might render cilia in mutant cells more labile to the application of serum. We applied serum to control and MTI-610-V-1 cells and scored the percentage of cells retaining a cilium, based on staining for acetylated tubulin and ARL13B at specific time intervals. By 4 h after serum application, wild-type cells had an 8% cilia withdrawal rate whereas INPP5E mutant cells had a 33% cilia withdrawal rate (73% versus 43%, $P < 0.01$; $n = 3$ independent experiments). At the 8-h and 24-h time points, the percentage of cells with visible cilia had equalized to about 40% in both the wild-type and mutant genotypes, suggesting that INPP5E controls the timing of cilia disassembly during early response to serum.

To determine whether the reduced number of ciliated mutant cells is due to an enhanced rate of cilia withdrawal in the absence of functional INPP5E, we performed scanning electron microscopy. Before the addition of serum, we found that the length of the primary cilium was approximately the same in control versus MTI-610-V-1 serum-starved fibroblasts, with both cilia measuring ~3 μm in length (**Fig. 4b–e**). However, at the 4-h time point (where we saw the maximal difference in cilia number), cilium length of the MTI-610 fibroblasts was about half of controls. These data were quantified in *x–y* sections from cells with remaining visible cilia as evidenced by immunostaining for ARL13B before the addition of serum and at 4 h and 8 h after serum addition. We found a significant decrease in average cilia length at 4 h after serum stimulation in mutant cells as compared to controls (2.73 versus 1.28 μm, wild-type versus MTI-610, $P < 0.01$; $n > 30$ cells for each condition), whereas no difference was apparent either before serum or after 8 h (**Supplementary Fig. 8**). Thus, ciliary disassembly is more rapid in the absence of full INPP5E activity compared with wild type.

Following ascertainment of fibroblast samples from additional affected individuals with *INPP5E* mutations, we noted some alterations in cell proliferation rates in culture and thus tested quiescent cells for the ability to reenter the cell cycle. Whereas MTI-610 fibroblasts had no apparent alteration in cell cycle reentry (based on Ki67 staining or BrdU incorporation), MTI-134 and MTI-627 showed a reduction in the percentage of mitotically active cells following serum addition (**Supplementary Fig. 9**). As MTI-134 and MTI-627 had more severe reduction in enzymatic activity than MTI-610 in the *in vitro* assay (0% and 8.5% versus 15%; **Fig. 2**), the data suggest that residual, but not full, function of INPP5E may be required for this serum-based cell cycle reentry. MTI-610 fibroblasts showed a normal percentage of mitotically active cells; however, a greater percentage of these mitotically synchronized cells reentered the cell cycle initially (Ki67 staining between 18–24 h) and progressed through the cell cycle more rapidly (reduction of BduU incorporation from 24 h to 30 h) than control fibroblasts, suggesting that INPP5E enzymatic activity may also influence the rate of cell cycle progression. Not all serum-based responses were abnormal in the samples from family MTI-610, however. For instance, there were no alterations in low-dose serum–dependent scratch-wound assay healing (**Supplementary Fig. 10**), which we designed to be migration dependent but largely proliferation independent[16]. We conclude that INPP5E

may play specific serum-dependent cellular roles, mediating both ciliary stability and cell cycle dynamics.

Our data show that hypomorphic mutations in *INPP5E* cause Joubert syndrome, providing the first evidence of a link between PtdIns signaling and ciliopathies. It will be important to determine whether the developmental defects observed in Joubert syndrome are the result of defects in cilia maintenance or are due to a more broadly defined disruption in PtdIns signaling. Because the PDGFαα receptor has been localized to primary cilia[17], and because PDGF is one of the key serum-derived factors that mediates cilia withdrawal concurrent with cell cycle reentry[18], it is possible that PDGF and other factors that use cilia as signaling centers have downstream pathways that are regulated through specific localization and function of INPP5E.

Previous studies have hinted at possible connections between PtdIns signaling and the cilium. Tubby mutant mice have phenotypes consistent with ciliary dysfunction, and the protein encoded by the mutated gene binds specific PtdIns, including PtdIns3,4,5(P3)[19]. Furthermore, Bardet-Biedl syndrome shares similar ciliopathy features with Joubert syndrome, and the Bardet-Biedl syndrome–linked protein BBS5 can bind PtdIns[9]. However, to our knowledge, our findings are the first to directly implicate defective enzymatic conversion within the PtdIns class with ciliary dysfunction. The fact that INPP5E displays enrichment within the ciliary axoneme makes it tempting to speculate that PtdIns signaling may not just function to regulate cilia stability but may also occur within the cilium. An alternative model is that INPP5E might be sequestered within the cilium but exert its activity within the cytoplasm, similar to the models being proposed for Sonic hedgehog signaling[20]. The identification of a key regulatory enzyme in this process highlights an important area of research with clinical relevance.

METHODS

Methods and any associated references are available in the online version of the paper at http://www.nature.com/naturegenetics/.

Note: Supplementary information is available on the Nature Genetics website.

ACKNOWLEDGMENTS

We thank the Marshfield Clinic Research Foundation, Center for Inherited Disease Research and University of California Los Angeles Microarray Core (supported by the US National Heart, Lung, and Blood Institute and National Institutes of Health) for genotyping support. J. Meerloo at the University of California San Diego (UCSD) Neuroscience Microscopy Imaging Core (P30NS047101) provided imaging support. Ryan Anderson of the UCSD Material Sciences provided electron microscopy support. We thank members of the the Dixon lab (UCSD) for suggestions and help with protein modeling, and members of the Mitchell lab (Monash University) for reagents. This work was supported by the UCSD Neuroplasticity of Aging Training Grant (to S.L.B.), the Italian Ministry of Health (RC2008 to B.D., Ricerca Finalizzata 2006 to E.M.V.), the Telethon Foundation Italy (GGP08145 to E.B. and E.M.V.), National Institutes of Health grant HL 16634 (to P.W.M. and M.V.K.), American Heart Association grant 0730350N (to M.V.K.), the National Institute of Neurological Disorder and Stroke, the Burroughs Welcome Fund, the March of Dimes and the Howard Hughes Medical Institute (to J.G.G.).

AUTHOR CONTRIBUTIONS

S.L.B, J.L.S, F.B., L.C.S., L.T., S.G., M.J., S.S. and M.V.K. performed experiments. L.A.-G., L.S., M.S.Z, A.A.-A., O.R., H.K., D.S., L.C.S., E. Bertini, E. Boltshauser and E.F. identified and recruited patients. R.A.B. shared unpublished data and reagents. S.J.F., B.D. and P.W.M. provided advice and helped with data interpretation. S.L.B and J.L.S assembled the figures. S.L.B, E.M.V. and J.G.G. wrote and edited the manuscript.

Published online at http://www.nature.com/naturegenetics/.
Reprints and permissions information is available online at http://npg.nature.com/reprintsandpermissions/.

1. Vicinanza, M., D'Angelo, G., Di Campli, A. & De Matteis, M.A. Phosphoinositides as regulators of membrane trafficking in health and disease. *Cell. Mol. Life Sci.* **65**, 2833–2841 (2008).
2. Valente, E.M., Brancati, F. & Dallapiccola, B. Genotypes and phenotypes of Joubert syndrome and related disorders. *Eur. J. Med. Genet.* **51**, 1–23 (2008).
3. Saar, K. *et al.* Homozygosity mapping in families with Joubert syndrome identifies a locus on chromosome 9q34.3 and evidence for genetic heterogeneity. *Am. J. Hum. Genet.* **65**, 1666–1671 (1999).
4. Valente, E.M. *et al.* Distinguishing the four genetic causes of Joubert syndrome-related disorders. *Ann. Neurol.* **57**, 513–519 (2005).
5. Tsujishita, Y., Guo, S., Stolz, L.E., York, J.D. & Hurley, J.H. Specificity determinants in phosphoinositide dephosphorylation: crystal structure of an archetypal inositol polyphosphate 5-phosphatase. *Cell* **105**, 379–389 (2001).
6. Kong, A.M. *et al.* Phosphatidylinositol 3-phosphate (PtdIns3P) is generated at the plasma membrane by an inositol polyphosphate 5-phosphatase: endogenous PtdIns3P can promote GLUT4 translocation to the plasma membrane. *Mol. Cell. Biol.* **26**, 6065–6081 (2006).
7. Kisseleva, M.V., Cao, L. & Majerus, P.W. Phosphoinositide-specific inositol polyphosphate 5-phosphatase IV inhibits Akt/protein kinase B phosphorylation and leads to apoptotic cell death. *J. Biol. Chem.* **277**, 6266–6272 (2002).
8. Jiang, X.R. *et al.* Telomerase expression in human somatic cells does not induce changes associated with a transformed phenotype. *Nat. Genet.* **21**, 111–114 (1999).
9. Nachury, M.V. *et al.* A core complex of BBS proteins cooperates with the GTPase Rab8 to promote ciliary membrane biogenesis. *Cell* **129**, 1201–1213 (2007).
10. Cantagrel, V. *et al.* Mutations in the cilia gene *ARL13B* lead to the classical form of Joubert syndrome. *Am. J. Hum. Genet.* **83**, 170–179 (2008).
11. Caspary, T., Larkins, C.E. & Anderson, K.V. The graded response to Sonic hedgehog depends on cilia architecture. *Dev. Cell* **12**, 767–778 (2007).
12. Alieva, I.B., Gorgidze, L.A., Komarova, Y.A., Chernobelskaya, O.A. & Vorobjev, I.A. Experimental model for studying the primary cilia in tissue culture cells. *Membr. Cell Biol.* **12**, 895–905 (1999).
13. Higginbotham, H., Bielas, S., Tanaka, T. & Gleeson, J.G. Transgenic mouse line with green-fluorescent protein-labeled Centrin 2 allows visualization of the centrosome in living cells. *Transgenic Res.* **13**, 155–164 (2004).
14. Chizhikov, V.V. *et al.* Cilia proteins control cerebellar morphogenesis by promoting expansion of the granule progenitor pool. *J. Neurosci.* **27**, 9780–9789 (2007).
15. Tucker, R.W., Pardee, A.B. & Fujiwara, K. Centriole ciliation is related to quiescence and DNA synthesis in 3T3 cells. *Cell* **17**, 527–535 (1979).
16. De Donatis, A. *et al.* Proliferation versus migration in platelet-derived growth factor signaling: the key role of endocytosis. *J. Biol. Chem.* **283**, 19948–19956 (2008).
17. Schneider, L. *et al.* PDGFRαα signaling is regulated through the primary cilium in fibroblasts. *Curr. Biol.* **15**, 1861–1866 (2005).
18. Pugacheva, E.N., Jablonski, S.A., Hartman, T.R., Henske, E.P. & Golemis, E.A. HEF1-dependent Aurora A activation induces disassembly of the primary cilium. *Cell* **129**, 1351–1363 (2007).
19. Santagata, S. *et al.* G-protein signaling through tubby proteins. *Science* **292**, 2041–2050 (2001).
20. Rohatgi, R. & Scott, M.P. Arrestin' movement in cilia. *Science* **320**, 1726–1727 (2008).

ONLINE METHODS

Research subjects. Twenty-seven consanguineous families from the Middle East, Turkey and Europe were included in this study based upon the following criteria: (i) at least one individual in the family with a neuroradiographically proven 'molar tooth sign' associated with any Joubert syndrome or related disorder phenotype; (ii) evidence for linkage to the *JBTS1* locus; (iii) exclusion of linkage to any other of the known JBTS loci (*JBTS2-9*). Whenever possible, patients underwent a full diagnostic protocol as previously reported[21]. Brain MRI analysis was completed during the clinical assessment using standard sequence protocols. Parental written informed consent was obtained from all families, and the study was approved by the Human Research Protection Program Committees of UCSD (La Jolla) and CSS-Mendel Institute (Rome).

Genome-wide screen and fine mapping of the *JBTS1* locus. A 5K whole genome linkage scan was performed in all informative families using the Illumina Linkage IVb mapping panel[22] and analyzed with easyLINKAGE-Plus software[23], which runs Allegro version 1.2c in a PC Windows interface to calculate multipoint lod scores. Parameters were set to autosomal recessive with full penetrance and disease allele frequency of 0.001. Fine mapping on selected individuals was performed with the Affymetrix 250K *Nsp*I SNP array and results were analyzed using pedigree-free identity by descent mapping. Short tandem repeat polymorphic markers at the *JBTS1* locus were used as previously published[4].

Mutation screening. Mutations were screened using a combination of single-stranded conformational polymorphism analysis and direct sequencing as described[24,25].

Bioinformatics. Protein evolutionary conservation was determined by aligning amino acids from the Human Genome Browser (http://www.genome.ucsc.edu). The ciliary proteome was searched using web-based tools[26,27]. Protein folding and intermolecular interactions were predicted using Swiss-Model with crystallized PtdIns 5-phosphatase domain of synaptojanin bound to Ca^{2+} and PtdIns(1,4)P2 (ref. 5). The resulting INPP5E structure was manipulated with PyMOL software by importing amino acid sequence for wild-type and mutant and comparing the likely docking site for PtdIns.

Biochemical assays. *INPP5E* cDNA[7] was cloned in-frame with enhanced GFP into pcDNA3.0 for expression. Mutations corresponding to those in the affected individuals were individually engineered into the *INPP5E* cDNA in a Myc-tagged vector and were then stably transfected into 293T cells using the T-Rex tetracycline-regulated system (Invitrogen)[7], immunoprecipitated using a Myc tag, confirmed by protein blot to each express comparable amounts (**Supplementary Fig. 3**) and then used in a modified PtdIns(4,5)P2 hydrolysis assay as described[28]. PtdIns(3,4,5)P3 hydrolysis was measured by adding purified substrate to the immunoprecipitates at 37 °C for 10 min, followed by malachite green for an additional 10 min[29]. Released inorganic phosphate was measured at 650 nm, compared against a standard curve, and performed in triplicate. Assessment of PtdIns(4,5)P2/PtdIns(4)P ratio from patient primary cells were metabolically labeled and performed as described[30]. Stably transfected 293T cells were stimulated with 50 ng/ml of PDGF and analyzed for Akt signaling as described[7].

Histology. Mouse tissues from wild-type or GFP-*Cent2* mice were immunostained with an affinity-purified peptide-specific INPP5E rabbit antiserum that reacts with human and mouse as reported[31] at 1:200. Images were acquired on a DeltaVision imaging system with 5–10 cycles of deconvolution.

Fibroblasts assay. Primary skin fibroblasts from affected and unaffected passage-matched control were grown at similar confluence for 3 d in the absence of serum. Ciliary disassembly and wound healing was assessed as described[18,32]. Cell cycle reentry was interrogated as described[33] with 20% serum addition to subconfluent fibroblasts. BrdU (10 μM) was applied for 1 h, and antigens were detected with antibodies to Ki67 (1:1,000) and BrdU (1:1,500) (Abcam nos. ab66155 and ab6326).

Scanning electron microscopy. Fibroblasts were fixed in 2.5% glutaraldehyde/0.1 M cacodylate buffer (CB) (pH 7.4) for 30 min at 25 °C, rinsed (0.1 M CB), postfixed (1% OsO_4/0.1 M CB) for 30 min at 4 °C, dehydrated with a graded alcohol series, which was displaced with hexamethyldisilazane, and evaporated overnight; samples were then sputter coated with palladium and imaged on XL30 ESEM-FEG.

Cilia length quantification. Cilia length was correlated in the *x-y-z* versus *x-y* using the Volocity rendering software. 3D reconstruction of cilia using DeltaVision imaging system with 100× objective with 0.1-μm *z*-steps allowed for length assessment irrespective of angle of orientation. Cilia length was also measured in the same cells using *x-y* only projections, and measurements were compared for five cells. No observable difference in cilia length measurements were detected, and thus subsequent lengths were measured from *x-y* projections.

GenBank accession numbers. Human *INPP5E* is assigned GenBank number NM_019892, and the encoded protein NP_063945. There is one minor splice variant annotated in human (U45974) due to a deletion of the 3′ stop codon, resulting in an additional 50 amino acids of the C-terminal protein. This stretch has no similarity in the database and is of unknown function.

21. Valente, E.M. *et al. AHI1* gene mutations cause specific forms of Joubert syndrome-related disorders. *Ann. Neurol.* **59**, 527–534 (2006).
22. Murray, S.S. *et al.* A highly informative SNP linkage panel for human genetic studies. *Nat. Methods* **1**, 113–117 (2004).
23. Hoffmann, K. & Lindner, T.H. easyLINKAGE-Plus—automated linkage analyses using large-scale SNP data. *Bioinformatics* **21**, 3565–3567 (2005).
24. Gleeson, J.G. *et al.* Genetic and neuroradiological heterogeneity of double cortex syndrome. *Ann. Neurol.* **47**, 265–269 (2000).
25. Valente, E.M. *et al.* Mutations in *CEP290*, which encodes a centrosomal protein, cause pleiotropic forms of Joubert syndrome. *Nat. Genet.* **38**, 623–625 (2006).
26. Inglis, P.N., Boroevich, K.A. & Leroux, M.R. Piecing together a ciliome. *Trends Genet.* **22**, 491–500 (2006).
27. Gherman, A., Davis, E.E. & Katsanis, N. The ciliary proteome database: an integrated community resource for the genetic and functional dissection of cilia. *Nat. Genet.* **38**, 961–962 (2006).
28. Caldwell, K.K., Lips, D.L., Bansal, V.S. & Majerus, P.W. Isolation and characterization of two 3-phosphatases that hydrolyze both phosphatidylinositol 3-phosphate and inositol 1,3-bisphosphate. *J. Biol. Chem.* **266**, 18378–18386 (1991).
29. Vandeput, F., Backers, K., Villeret, V., Pesesse, X. & Erneux, C. The influence of anionic lipids on SHIP2 phosphatidylinositol 3,4,5-trisphosphate 5-phosphatase activity. *Cell. Signal.* **18**, 2193–2199 (2006).
30. Zhang, X., Hartz, P.A., Philip, E., Racusen, L.C. & Majerus, P.W. Cell lines from kidney proximal tubules of a patient with Lowe syndrome lack OCRL inositol polyphosphate 5-phosphatase and accumulate phosphatidylinositol 4,5-bisphosphate. *J. Biol. Chem.* **273**, 1574–1582 (1998).
31. Kisseleva, M.V., Wilson, M.P. & Majerus, P.W. The isolation and characterization of a cDNA encoding phospholipid-specific inositol polyphosphate 5-phosphatase. *J. Biol. Chem.* **275**, 20110–20116 (2000).
32. Rodriguez, L.G., Wu, X. & Guan, J.L. Wound-healing assay. *Methods Mol. Biol.* **294**, 23–29 (2005).
33. Kim, J., Krishnaswami, S.R. & Gleeson, J.G. CEP290 interacts with the centriolar satellite component PCM-1 and is required for Rab8 localization to the primary cilium. *Hum. Mol. Genet.* **17**, 3796–3805 (2008).

doi:10.1038/ng.423